Carbon supported NiRu nanoparticles as effective hydrogen evolution catalysts for anion exchange membrane water electrolyzers

Ruck, S.; Körner, A.; Hutzler, A.; Bierling, M.; Gonzalez, J.; Qu, W.; Bock, C.; Thiele, S.; Peach, R.; Pham, C. V.

Publisher's version / Version de l'éditeur:
https://doi.org/10.1088/2515-7655/ac95cd
Journal of Physics: Energy, 4, 4, 2022-10-14

Journal of Physics: Energy

OPEN ACCESS

RECEIVED
26 August 2022

REVISED
20 September 2022

ACCEPTED FOR PUBLICATION
28 September 2022

PUBLISHED
14 October 2022

PAPER

Carbon supported NiRu nanoparticles as effective hydrogen evolution catalysts for anion exchange membrane water electrolyzers

S Ruck[1,2,*], A Körner[1,2], A Hutzler[1], M Bierling[1,2], J Gonzalez[1,2], W Qu[3], C Bock[3], S Thiele[1,2], R Peach[1] and C V Pham[1,*]

[1] Helmholtz-Institute Erlangen-Nürnberg for Renewable Energy (IEK-11), Forschungszentrum Juelich GmbH, Erlangen, Germany
[2] Department of Chemical and Biological Engineering, Friedrich-Alexander Universität Erlangen-Nürnberg, Erlangen, Germany
[3] Department of Energy, Mining and Environment, National Research Council Canada, Vancouver, Canada
[*] Authors to whom any correspondence should be addressed.

E-mail: s.ruck@fz-juelich.de and c.pham@fz-juelich.de

Keywords: nickel, ruthenium, carbon supported, catalyst, HER, anion exchange membrane, electrolysis

Supplementary material for this article is available online

Abstract

Establishing anion exchange membrane water electrolysis (AEMWE) as a new technology for efficient hydrogen production requires cost-effective and high-performance catalyst materials. Here, we report the synthesis and comprehensive characterization of carbon supported NiRu alloy nanoparticles as a cost-effective hydrogen evolution reaction catalyst for AEMWEs. Different NiRu catalysts were synthesized using a facile and scalable impregnation method. Half-cell results showed the 'NiRu' catalyst with ca. 10 wt.% Ru to exhibit an increased noble metal mass activity and slightly decreased Tafel slope compared to a commercial Pt/C catalyst with 60 wt.% Pt. Further, we report the application of NiRu/C as a cathodic catalyst in AEMWE full cell for the first time. In full cell tests, the synthesized catalysts exhibit 2 A cm^{-2} at 1.95 V with a low loading of 0.1 mg_{PGM} cm^{-2} at the cathode.

1. Introduction

Hydrogen is one of the most promising energy carriers for sustainable energy systems. Efficient production of hydrogen by utilizing renewable energy sources is essential for establishing a hydrogen-powered energy landscape [1–4]. One of the emerging technologies considered as most promising to produce hydrogen at reduced cost is the anion-exchange-membrane water electrolyzer (AEMWE). Advantages of this technology include the possibility to utilize non-noble catalyst materials in alkaline media with a compact zero-gap design similar to the more mature proton-exchange-membrane water electrolyzer [5–8]. More specifically, the use of transition metals as oxygen evolution reaction catalysts have been shown to achieve comparable performances to IrO_2 in alkaline conditions offering the prospect of lowering AEMWE cost [9–11]. However, the activity and stability of platinum for the hydrogen evolution reaction (HER) remain unrivaled in both acidic and alkaline media. Hence, the costly Pt is still of high interest for electrolysis applications [12]. The use of Pt as the dominant catalyst material for high-performance electrolyzers remains a significant problem due to its high cost and scarcity [13, 14]. Nickel shows the best non-noble activity for the HER in alkaline media [15, 16]. Still, its performance is insufficient to enable application as an alternative to Pt-based catalysts for zero gap water electrolyzers, and therefore calls for the need of further development. An alternative approach is to alloy different metals (noble and non-noble) to lower the amount of noble metal in the catalyst material while maintaining a high activity [17–22].

Recent studies report the combination of nickel and ruthenium as HER catalysts with superior activity in alkaline environments. The creation of bimetallic surfaces and the accompanying electronic interactions are shown to result in a shift of the d-band center and optimized binding energies towards atomic hydrogen in alkaline conditions [23–27]. Therefore, it is assumed that combining both metals increase the HER activity

due to the correlation of volcano theory and HER activity. The design of state-of-the-art electrocatalysts relies on high activity, high electrical conductivity, and high surface area of the catalyst (in other words the intrinsic catalytic activity). These requirements can be fulfilled by creating a catalyst with metal nanoparticles (NPs) supported on a highly porous carbon-based material. This catalyst design is frequently used in high-performance electrolysis and fuel cell applications due to high surface area and good electric conductivity and can therefore be used as stable and well-known reference material. The choice of carbon support materials does play a crucial role in the catalyst's performance due to their conductivity, stability and morphology [28]. Latest studies report on different approaches to apply complex carbon structures like carbon nanotubes or encapsulated active sites. These studies show that NiRu alloys can be a cost-effective alternative to Pt as the Ru price is more than 40% lower than Pt in the past 5 years [29]. In anion exchange membrane fuel cells, NiRu/C showed superior performance in three-electrode set-ups and full cell tests, reported by Xue *et al* [29]. Li *et al* [30] reported superior activity of RuNi NPs embedded in N-doped carbon nanofibers as HER catalyst in alkaline media which outperforms 20 wt.% Pt/C. Liu *et al* [31] showed Ni–Ru nanoalloys encapsulated in mesoporous carbon as solid HER catalyst and Peng *et al* [25] reported NiRu nanoalloys attached to multiwalled carbon nanotubes with good performance in alkaline and acidic media.

In most studies, catalyst performance is evaluated using a three-electrode set-up with a rotating disk electrode (RDE). Especially HER activity data reported in literature are more difficult to compare due to different set ups, catalyst layer (CL) preparation and the sensitivity of this technique regarding inaccuracies and impurities. Aforementioned studies showed very promising activities of NiRu alloys catalysts in three electrode set-ups. Moreover, since Ru is lower in price than Pt, NiRu alloy could be an alternative to the incumbent Pt catalysts. However, this class of catalysts has not yet been investigated in full cell membrane electrode assembly (MEA) characterizations. It is however accepted that testing new catalysts in MEA full cell is an important measure to evaluate the catalyst's activity and stability in the real operating system including the liquid (electrolyte) and gaseous reactant effects. It is known that superior activity in half cell experiments might not be transferable into the full cell performance. In an MEA the electrocatalyst is required to form electronically and ionically conductive networks without hindering the flow of reactants [32]. In this paper, we study the synthesis and electrochemical performances of NiRu NPs supported on high surface area carbon (NiRu/C). Both half-cell and full cell MEA set-ups are utilized for the studies.

The synthesized catalysts were characterized by employing several techniques to evaluate the structure and chemical composition of the materials. High angle annular dark field scanning transmission electron microscopy (HAADF-STEM) was used to determine the microscopic structure and particle size. Crystal morphology of the metal particles was analyzed by x-ray diffraction (XRD) and scanning electron microscopy (SEM). Electrochemical characterization was carried out by RDE experiments and MEAs were fabricated for full cell performance tests. In MEA full cell tests, the synthesized NiRu/C catalysts showed a favorable activity compared to a state-of-the-art Pt/C catalyst while using 0.1 mg_{Ru} cm^{-2} at the cathode.

2. Methods

2.1. Synthesis of NiRu/C electrocatalyst

NiRu/C catalysts were synthesized by an impregnation method and subsequent thermal H_2 reduction. For a 1 g batch of catalyst, 0.4 g of carbon (Ketjen Black, Fuel Cell Store) were added into a mixture of 75 ml water (MilliQ) and 75 ml isopropanol (Sigma Aldrich, 98%, technical grade) in a 250 ml round bottom flask and dispersed by ultrasonication for 20 min. Specific amounts (see table 1) of nickel(II) chloride hexahydrate (Sigma Aldrich) and ruthenium(III) chloride hydrate (Sigma Aldrich; 40 wt.% Ru) were added into the reaction mixture and stirred for 1 h. Next, the solvents were evaporated in a rotary evaporator (Büchi Rotavapor R-3000) and the dry powder was collected. Finally, the reduction reaction was carried out at 500 °C for 2 h under the flow of 5 vol.% H_2 in Ar in a tube furnace. The gas flow of 150 sccm was kept constant during both the heating (5° C min^{-1}) and cooling phase. Carbon supported catalysts of different atomic ratios of Ni to Ru (9:1, 8:2, 7:3) were synthesized in this manner.

2.2. Physical characterization

For structural and compositional analysis, STEM was carried out. A Talos F200i (Thermo Fisher Scientific) equipped with a Schottky field-emission gun (X-FEG) and a Dual Bruker XFlash 6 | 100 EDXS detector was used. Samples were plasma cleaned before imaging using a Tergeo-EM Plasma Cleaner (PIE Scientific). For spectrum imaging and (high-resolution) STEM (HRSTEM), a primary electron energy of 200 keV was used and the electron probe was tuned to a beam current of 41 pA and a convergence angle of 10.5 mrad. A HAADF detector was employed for collecting elastically scattered electrons towards an angular range of 58–200 mrad.

Table 1. Overview of different composition samples and used precursor amounts. The listed amounts are for a 1 g batch size with a total metal content of 60 wt.%, i.e. 0.4 g carbon support for each batch.

Sample description	Ni:Ru at. ratio	Ru content (wt.%)	$NiCl_2$ $6H_2O$ (g)	$RuCl_3$ H_2O (g)
NiRu/C 9:1	9:1	9.6	2.04	0.241
NiRu/C 8:2	8:2	18.0	1.69	0.451
NiRu/C 7:3	7:3	25.4	1.39	0.637

A scanning electron microscope (Crossbeam 540 with a Gemini II column, Zeiss) with an EDXS-detector (X-Max 150 silicon drift detector, Oxford Instruments; Software: Aztec Version 4.2, Oxford instruments) was used for structural and compositional analysis of the catalyst powder. Therefore, the catalyst powder was fixed on a SEM-stub with a conductive double-sided adhesive carbon pad. Surface imaging was performed at an accelerating voltage of 3 kV and a beam-current of 750 pA. A voltage of 30 kV and a current of 1 nA was applied to receive a compositional analysis of the powder.

Powder XRD patterns were recorded using a Bruker D8 advanced diffractometer, while applying a Cu-Kα radiation with a wavelength of 0.154 nm, using an angular step size of 0.02° 2Θ within an angular range of 15°–90°.

Furthermore, N_2 adsorption–desorption isotherms were recorded at 196 °C (SA 3100, Beckman Coulter) and the specific surface area was calculated using the Brunauer–Emmett–Teller (BET) method.

2.3. Electrochemical characterization

2.3.1. RDE studies

For the electrochemical characterization an RDE set-up from Pine Research was used with a glassy carbon RDE tip. Catalyst inks were prepared by dispersing 2.15 mg of catalyst powder in a 5 ml mixture of 1-propanol and water, (1:4 volume ratio) with 0.215 mg of ionomer (Aemion AP1-HNN8-00-X, dissolved in 1-propanol) acting as binder and ink stabilizer. The catalyst ink was ultrasonicated for 30 min. The CLs were prepared by drop-casting 10 μls of the ink onto the glassy carbon RDE tip. The catalyst ink was then left to dry for 30 min at room temperature prior to the electrochemical testing. The catalyst loading (metal plus carbon support) was kept constant at 22.2 μg cm^{-2} for all samples. An in-house designed Teflon cell was used with a Hg/HgO reference electrode (Ketlow) and a high surface area graphite rod as a counter electrode. In this work the potential of the Hg/HgO reference electrode was converted to the potential of the reversible hydrogen electrode (RHE) for ease of comparison to literature results. A Solartron SI 1287 potentiostat was used for the electrochemical measurements. For electrochemical activity evaluations, an activation step was applied before linear sweep voltage (LSV) curves were recorded. For the activation step, 2 min of constant current (10 mA cm^{-2} vs. RHE) hold was applied. After the activation step, the cell was paused for 15 min rotating to remove formed hydrogen gas before recording the LSV curves between 60 mV and −130 mV vs. RHE. The electrolyte was continuously purged with Ar gas at 200 ml min^{-1}, 1 h before and throughout the measurement to ensure O_2 and CO_2 were removed. The RDE was rotated at 1600 rpm in 1 M KOH for all measurements. For the stability tests a 1 cm^2 carbon paper was dip-coated with catalyst ink adapted from [33]. Therefore, the active area of the carbon paper was dipped and dried ten times into the same catalyst ink prepared before. The loading was determined by weighing the sample before and after the dip-coating and reached 0.1 mg cm^{-2}. The electrode was placed into the half-cell set-up, and a constant current measurement at 10 mA cm^{-2} was carried out for 20 h.

2.3.2. MEA fabrication and full cell test

All MEAs were fabricated with an active area of 5 cm^2, where a commercially available anion exchange membrane (AF1-HNN8-50-X, Ionomr) with 50 μm thickness, was sandwiched between the catalyst-coated electrodes. The ink for the cathode electrode was fabricated using 1 wt.% of total solids in 1-propanol and water (4:1) as solvents. First, the ionomer granulate (0.1 wt.% of total mass of final ink; Aemion AP1-HNN8-00-X, Ionomr) was dissolved in 1-propanol. Then water and catalyst (0.9 wt.% of total mass) were added to the solution. As reference material 60 wt.% Pt on Ketjen Black was used for all experiments (Fuel Cell Store). The ink was sonicated with an ultrasonic horn (Hielscher) at 40 W for 3 iterations of 20 min while cooling the ink in an ice bath. The anode ink was prepared as described elsewhere [34] using commercial IrO_2 (Alfa Aesar) as catalyst material but contained a lower amount of binder (0.02 wt.% AP1-HN8-00-X Ionomer purchased from Ionomr, and 0.98 wt.% of catalyst).

An ultrasonic spray coating process was adapted from Bühler *et al* [35], for fabrication of the electrodes. An ExactaCoat spray coater with an ultrasonic AccuMist nozzle (48 kHz) from SonoTek was used. Table S1 shows the technical parameters of the spray coating process.

The catalyst loading was determined by weighing the electrodes using a Sartorius Cubis microscale (MSA66S-000-DH). The anode electrode was fabricated by spray-coating the IrO_2 ink onto porous Ni substrates (BEKIPOR 2NI18-0.25, Beakert). The catalyst loading was kept constant for all experiments at 1.5 mg_{Ir} cm^{-2}. The cathode catalyst was sprayed on a gas diffusion layer (GDL) from Freudenberg (H24C5). While testing different cathode catalysts of varying metal compositions, the catalyst mass loading was changed. For comparison, the catalyst loading was normalized to the mass of the Pt group metal (PGM) per cm^2.

For the assembly, gaskets, with a punched-out square of 5 cm^2 held the electrodes in position. A square membrane of 36 cm^2 was punched out and sandwiched between the catalyst coated electrodes in its dry state. Gold-coated flow fields with a parallel flow pattern and copper current collectors were utilized. The endplates were screwed together with a torque of 5 Nm, sandwiching the MEA (see schematic MEA configuration in figure 4(d)). The full cell tests were carried out in an in-house-designed test station at 70 °C with 1 M KOH as electrolyte. The electrolyte volume flow was constant at 40 ml min^{-1}, and the electrolyte was preheated to maintain a constant operating temperature. A VMP3 Biologic potentiostat was used to perform the electrochemical tests.

The single cell testing procedure was started with 2 h of constant voltage holding at 1.8 V as break-in procedure. The break-in procedure was also needed as the membrane was mounted in the cell in the dry state, due to easier handling and less risk of membrane damaging. Pre-experiments showed similar behavior in the cell with some performance difference (larger high frequency resistance) to a pretreated membrane. This is likely caused by higher cell compression of the swollen (fully hydrated) state of the membrane (figure S6). Next, the polarization curve was recorded by a constant current held for 3 min at each current step to reach steady-state conditions. This step was followed by potential-electrochemical impedance spectroscopy in the activation region at 1.5 V with a holding time of 15 min before measurements was started. Furthermore, a Galvano-electrochemical impedance spectroscopy in the ohmic region at 1 A cm^{-2} and in the high current region at 3 A cm^{-2} was carried out. (A holding time of 15 min was applied before the start of measurements at each current density, amplitude 10% of DC current, 10 points per decade.)

3. Results and discussion

3.1. Physical characterization

Different techniques were applied to evaluate the synthesis route for the resulting catalyst structure, morphology, and chemical composition. To assess the microscopic structure of the synthesized NiRu/C catalysts HR-STEM was performed. Since the catalysts of this work adapt the design of a commercial 60 wt.% Pt/C catalyst, a similar particle size and coverage of the carbon support was utilized which was proven to be implemented successfully by HR-STEM of both catalyst materials (figure S1).

For further materials structure characterization, STEM-EDXS spectrum imaging was carried out to map the elemental distribution of the catalyst samples. The NiRu NPs are shown to be adhered and homogeneously distributed across the surface of the carbon support (figure S2), and the Ni and Ru elements were evenly distributed over the metal particles (figures 1(a)–(d)) STEM-EDXS analyses also revealed core–shell like structures of the NPs (figures 1(e) and (f)).

Figure 1(f) shows an EDXS line profile of a larger, 10 nm diameter catalyst particle. This indicated a Ru-enriched core and a Ni-enriched shell. Pingali *et al* [36] reported on similar structures from the synthesis of NiRu NPs utilizing a pyrolysis process. It was reported that larger intermolecular forces between the Ru atoms are responsible for the Ru-enriched core. Since the synthesis route used in our study differs, another explanation could be, that Ru^{3+} was reduced at lower temperatures than Ni^{2+} and formed the core due to earlier nucleation. However, further investigation would be necessary to clarify the mechanism of its formation, which is beyond the scope of this work.

The specific surface area was determined to quantify and to compare the structure of the synthesized catalyst materials. Nitrogen adsorption–desorption surface analysis was carried out using the BET method to calculate the specific surface area. The commercial Pt/C reference material showed a BET-surface area of 245 m^2 $g_{cat}{}^{-1}$ (600 m^2 $g_{carbon}{}^{-1}$), while the NiRu/C catalyst showed a measured BET surface of 264.46 m^2 $g_{cat}{}^{-1}$ (661.15 m^2 $g_{carbon}{}^{-1}$), (Isotherms in figure S4). Consequently, for both catalysts a similar surface area was found. Still, pristine Ketjen Black shows a significantly larger specific surface area of over 1300 m^2 g^{-1}. However, Rahman *et al* [37] reported that the BET surface area of Pt NPs supported on Ketjen Black decreases with increasing loading of metal particles due to the blocking of micropores. The surface analysis further showed that both materials have a comparable pore volume and distribution.

XRD analysis was performed to investigate the crystalline structure of synthesized metal NPs. XRD spectra of the catalyst powder samples showed peaks at $2\theta = 44.48°$, 51.72°, and 76.55°. Those peaks corresponded to Ni 111 (2.03 Å, lattice plane distance), 200 (1.77 Å), and 220 (1.24 Å), respectively [38].

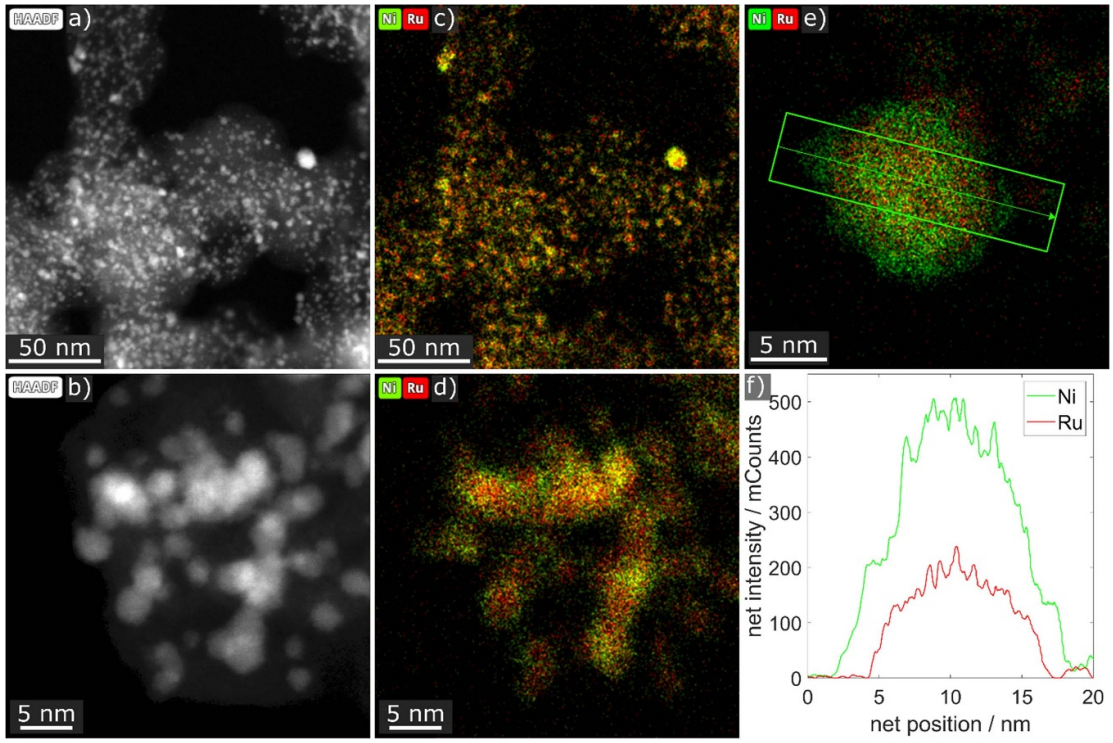

Figure 1. Structural STEM-EDXS analysis of NiRu/C catalyst with a calculated NiRu ratio of 9:1 in different magnifications: (a)–(d) STEM-EDXS analysis of NiRu/C catalyst material showed that both materials were present in nanoparticles and homogeneously distributed on the surface of the carbon support. (e), (f) EDXS line profile of a nanoparticle showing a core shell like structure. (See STEM-EDX results of all NiRu/C samples in figure S3.)

Moreover, two additional peaks emerged in samples with increasing Ru content (8:2, 7:3) at $2\theta = 39.21°$ ($\hat{=}$2.30 Å) and 42.6° ($\hat{=}$2.12 Å). Those emerging peaks are slightly shifted from Ru peaks at $2\theta = 38.45°$ ($\hat{=}$2.33 Å) and $2\theta = 42.22°$ ($\hat{=}$2.13 Å), indicating that Ru is alloyed.

SEM and STEM imaging indicated that besides the smaller particles, which contain Ni and Ru, the bulk material also contains larger Ni particles (figure S5) with diameters up to 0.8 μm. These large Ni dominated clusters in the bulk material can explain the prominent Ni peaks in the XRD spectra, outshining the contribution of smaller NPs. Small peaks in the XRD spectra of sample NiRu/C 7:3 (figure 2(a), peaks 1 and 2) fit well to lattice planes at 2.33 Å and 2.11 Å revealed by HR-STEM analysis of a single NP (figures 2(b) and (c)) and point towards alloyed NiRu NPs.

This shows that the proposed synthesis route from this study did not transfer the entire Ni precursor into NPs on the carbon support. A significant amount of the deposited metal forms large Ni particles in the bulk material, detached from the carbon support. This means that a percentage of the catalyst's total metal loading of 60 wt.% is not present as NPs on the carbon support surface. This heterogeneous distribution of Ni particles and NiRu NPs, is confirmed by SEM-EDXS analysis as well (figure S5). Unexpectedly, the measured BET surface of the NiRu/C sample was higher than that of the Pt/C reference. The increased BET surface can be explained by a lower NP coverage compared to the Pt/C sample. Hence, fewer micropores of the carbon support are blocked, which increases the measured BET area. Since Ni particles of larger size show comparably poor activity for the HER, the electrochemically active part of the catalyst is compromised as the desired design of the catalyst is not entirely reached. Consequently, the metal ratio of Ni and Ru within the NPs is expected to deviate from the anticipated values.

3.2. Electrochemical characterization

Electrocatalytic activity of the catalysts with different Ni/Ru ratios was first evaluated in a three-electrode set-up. Figure 3 a shows the LSV data for the investigated catalyst materials. A lower loading than typically reported in the literature [40] was chosen to form a thin CL on the glassy carbon tip. This improves the H_2 gas removal and decreases mass transport resistances to a minimum. All recorded measurements were carried out three times and showed good reproducibility (figure S7). Figure 3(b) shows the calculated Tafel plots. The recorded overpotentials of the synthesized NiRu/C catalyst are between 103–110 mV at 10 mA cm^{-2} while showing Tafel slopes between 71–74 mV dec^{-1}, which are slightly decreased compared to those of commercial Pt/C (89 mV @ 10 mA cm^{-2}; 66 mV dec^{-1}). The catalytic activity in the microkinetic

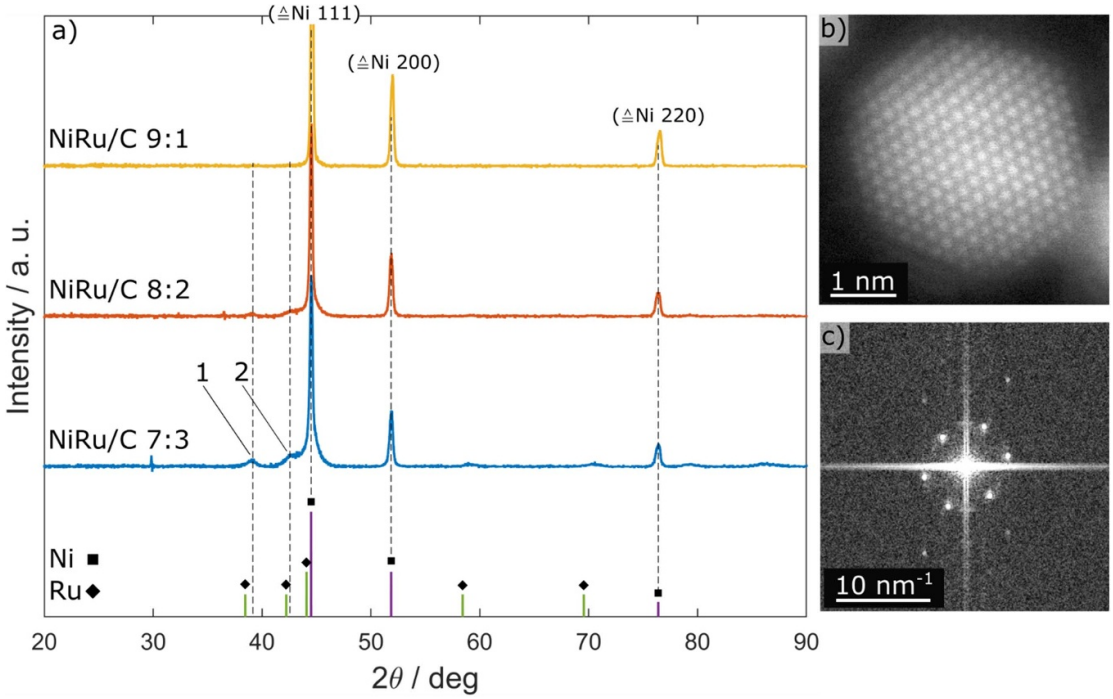

Figure 2. (a) XRD patterns of NiRu/C catalyst samples and Ni and Ru [38, 39]; (b) HAADF-HRSTEM micrograph of an individual nanoparticle and (c) its corresponding diffractogram (FFT).

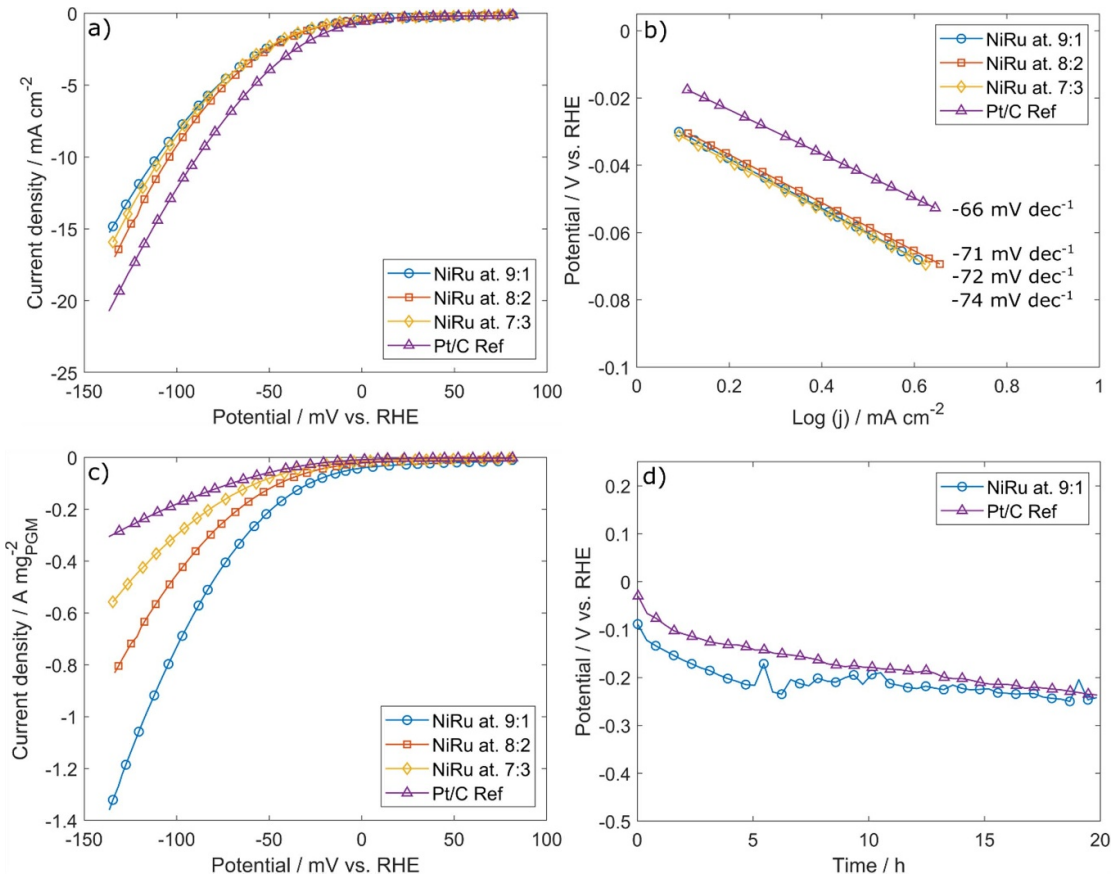

Figure 3. Catalytic activity of NiRu/C catalysts with different Ni/Ru ratios in RDE measurements in 1 M KOH at 1600 rpm and 10 mV s^{-1}; catalyst loading (total solids) of 22 μg cm^{-2}; (a) recorded LSV curves (error bars are smaller than data points); (b) calculated Tafel slopes; (c) PGM normalized LSV curves; (d) 20 h constant current stability test in three-electrode setup at 10 mA cm^{-2}.

region does not seem to show a strong dependence on the Ni/Ru ratio, but a dependence is seen at higher current densities. Nevertheless, the catalysts synthesized in this work exhibit significantly higher PGM mass activity than the commercial Pt/C as shown in figure 3(c). It is worth noting that a total PGM (Ru) content of NiRu/C is 9.6–25.4 wt.% (Ni:Ru at.: 9:1 = 9.6 wt.%; 8:2 = 18 wt.%; 7:3 = 25.4 wt.%), which is considerably lower than 60 wt.% of commercial Pt/C. This indicates that the activity of the structurally not optimized NiRu/C catalyst may outperform the commercial Pt/C catalyst by increasing the catalyst loading. As shown in the physical characterization (figure S5), the synthesized catalysts were not structurally optimized, as some undesired large Ni particles existed, which influence the measurement drastically due to a higher and lower surface area. Figure 3(d) presents a simple stability test by constant current hold at 10 mA cm^{-2} for 20 h. The investigated catalyst material showed comparable stability over 20 h with commercial Pt/C catalyst under simplified conditions. The NiRu catalysts tend to accumulate large H_2 gas bubbles. The bubble formation and removal within the electrode caused the fluctuation of the curve of NiRu/C catalyst. Whereas, the removal of gas bubbles from Pt/C electrode was favorable, thus the curve was smoother, compared to that of NiRu/C catalysts. Full MEA durability investigations over extended time periods should be performed in future works to investigate the catalysts stability under operating conditions.

3.3. Full cell performance test

As described earlier, half-cell measurements alone cannot evaluate the activity of a catalyst material in a real electrolyzer system. It is crucial to investigate the behavior of a new catalyst in a full MEA. Therefore, a MEA for every catalyst sample was fabricated as described in 2.3.2 and tested with 1 M KOH as electrolyte. We choose 1 M KOH as electrolyte to carry out the experiments for proper comparison with previous studies in the literature, since most of which use this electrolyte. Further, a lower KOH concentration is less harmful for the cell hardware and membrane materials. Figure 4 presents the polarization data of the MEA full cells utilizing NiRu/C catalysts with different Ni/Ru ratios on the cathode. From the full cell measurements, it was concluded that the NiRu/C 9:1 ratio shows the best performance among the NiRu/C catalyst ratio's synthesized (figure 4(a)). The cell reached a current density of 2 A cm^{-2} at 1.95 V. This is a notably high performance compared to the reported results from literature with Pt/C cathodes tested in comparable conditions [41–47]. A more detailed classification of the reported performance compared to literature data is provided in table S2. Moreover, the comparison of full MEA performance data from the literature to evaluate a synthesized HER catalyst is rather difficult due to several reasons. The anode side is considered limiting in electrolysis applications (slower kinetics). Therefore, the comparability of the anode is important to consider. Further, the used ionomer and membrane polymer has a great influence on the cell's performance. Under consideration of these parameters (1.75–1.9 V @ 1 A cm^{-2}) our catalyst's performance is on the top of reported literature.

For the full cell tests with loading of 0.1 mg_{Ru} cm^{-2} on the cathode, the performance of the NiRu/C (9:1) catalyst was comparable to that of the commercial Pt/C catalyst of similar PMG loading of 0.1 mg_{Pt} cm^{-2} (figure 4(a)). The activity data (figure 3) recorded in the half-cell experiments indicate that NiRu/C could outperform Pt/C if a higher catalyst loading is used. At this point it is clear that this activity/performance could not be transferred to full cell applications.

One main difference between RDE and full cell experiments is the effect of mass transport. Thus, for comparing the performance of a catalyst among other catalysts or to a state of the art catalysts the morphologies of the CLs must be comparable (such as thickness, porosity, etc). Since both catalyst systems have a similar microscopic design, ink preparation and CL fabrication were kept similar for this study. The SEM images in figure 5 show that the spray-coated CL of the NiRu/C samples was much more compressed compared to the platinum electrode, which offers a very porous surface and with a hierarchical pore structure. However, higher magnifications showed that the microscopic structure of the catalyst materials remained similar in the CL. High-frequency resistance (HFR) data were collected within the impedance measurement as described in 2.3.2 in order to help evaluate the MEA's electrical resistance and was used to calculate the HFR-corrected polarization curves, which represent the cell performance normalized on internal ohmic resistances. The HFR-corrected polarization curves show the same behavior as the half-cell measurements at low current densities (figure 4(c)), and NiRu/C 9:1 exhibited the best performance among the NiRu/C catalysts. The NiRu/C 9:1 catalyst showed comparable activity with Pt/C in the kinetic region. When current densities were increased, exceeding 0.75 A cm^{-2}, NiRu/C 9:1 outperformed the Pt/C counterpart. The blocking of active sites through gas bubbles can be excluded based on the morphology similarity of the Pt/C electrode and NiRu/C 9:1 electrode (figures 5(b) and (d)). Therefore, the better activity of NiRu/C 9:1 in the high current density range can be explained by larger amount of active sites contributed by Ni sites added to Ru sites within the electrode. This is also consistent with RDE data as NiRu/C 9:1 showed higher PGM mass activity than Pt/C.

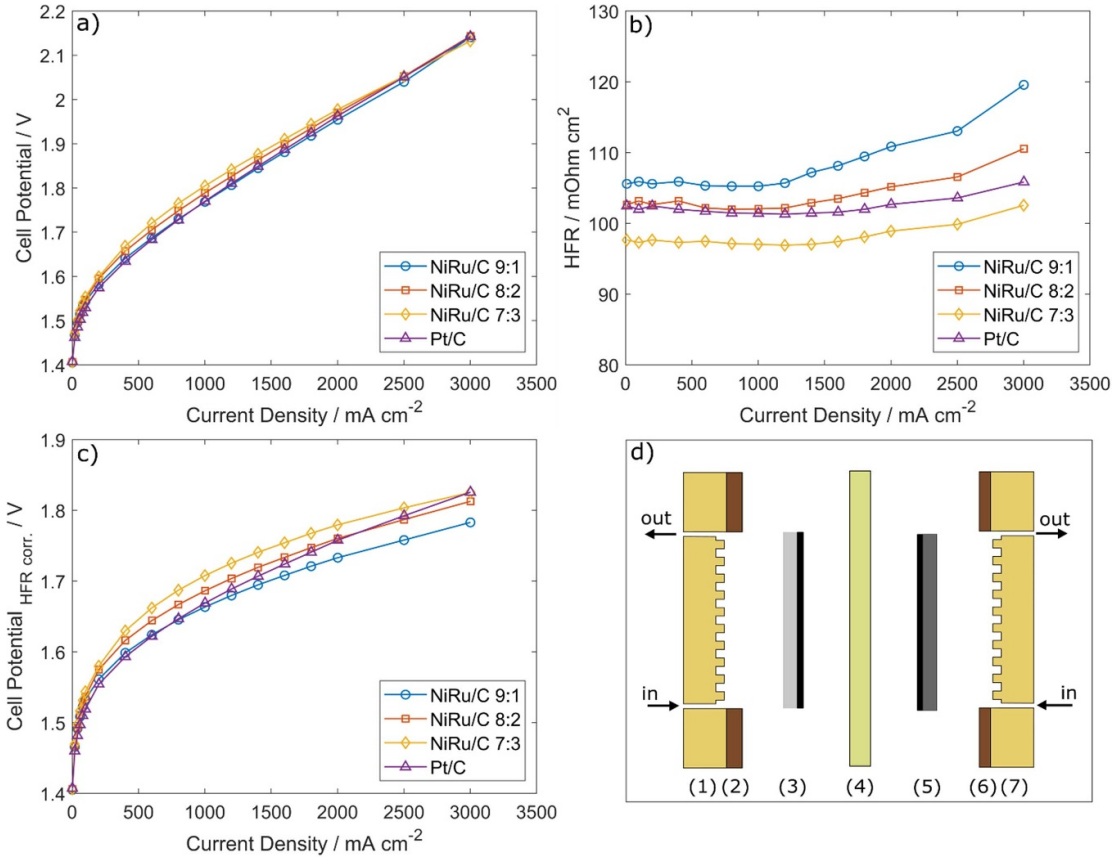

Figure 4. Polarization curves of full cell test. NiRu/C electrodes with 0.1 mg_{Ru} cm^{-2}; Pt/C electrode with 0.1 mg_{Pt} cm^{-2}; (a) as recorded polarization curves (error bars shown in SI for the sake of clarity); (b) HFR data; (c) HFR-corrected polarization curves; (d) MEA configuration: (1), (7): flow fields; (2), (6): gaskets; (3): spray coated IrO_2 catalyst layer on sintered Ni fibers as anode; (4): 50 μm Aemion membrane; (6): spray coated catalyst layer containing investigated catalysts (Pt/C, NiRu/C) on Freudenberg GDL.

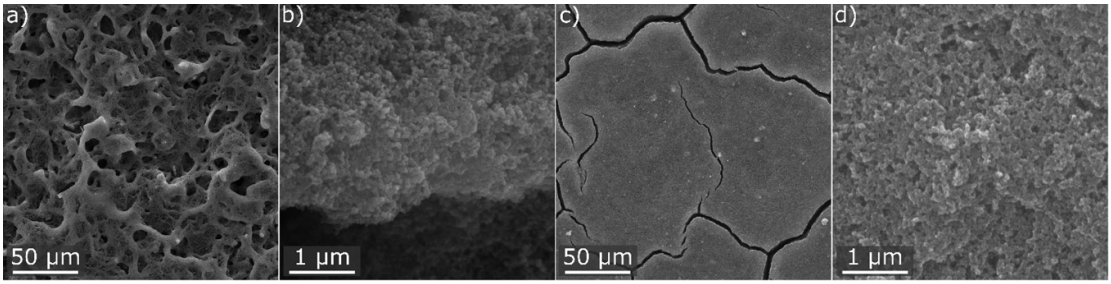

Figure 5. Spray coated electrodes (parameters in table 1). (a), (b) Pt/C reference, 0.1 mg_{Pt} cm^{-2} (0.16 mg_{cat} cm^{-2}); (c), (d) NiRu/C 9:1, 0.1 mg_{Ru} cm^{-2} (1.04 mg_{cat} cm^{-2}).

The HFR data (figure 4(b)) of the NiRu/C electrodes however showed that with increasing catalyst loading, the HFR increased; accordingly, this can be contributed to thicker CLs and their increased electrical resistance. The HFR of the Pt/C CL has an approximately 105 mOhm cm^2 resistance at high frequencies, which is intermediate compared to the NiRu/C electrodes with higher thickness. Since the HFR is affected by electric resistance, pore volume and ionic resistance of the CL, by other means its macroscopic structure plays a crucial role. The remarkable difference in electrode morphology shows that even minimal changes in the catalyst material can lead to significant differences in the spray coating behavior of the catalyst materials. It indicates that spray-coated CLs and their inks, respectively, should be optimized for every catalyst material to establish a trade-off between catalyst loading (thickness) and macroscopic porosity (contact resistance vs. mass transport issue). This shows once more that the conversion of half-cell activity results to full cell performance is not straightforward.

4. Conclusions

A catalyst based on NiRu alloy NPs supported on carbon was designed and successfully synthesized in this work. According to STEM investigations, NiRu/C had similar morphology in terms of particle size and coverage on the carbon support to a state-of-the-art Pt/C catalyst, that is favorable for electrolysis applications. A simple synthesis route was established based on a wet impregnation method, which is scalable. STEM and SEM analysis reveal that the NiRu/C catalysts comprising NiRu alloy NPs with diameters of 3–10 nm, covering the carbon support surface homogeneously. However, a part of the reduced metal (mainly Ni) was forming large particles with diameters up to 0.8 μm detached from the carbon support. Consequently, the Ni/Ru metal ratio of the NPs and the desired structure is not fully reached, which make room for further synthesis optimization.

Both half-cell and full cells results showed that NiRu/C with lower Ru content (Ni:Ru = 9:1) exhibited best PGM mass activity (i.e. noble metal utilization). In MEA full cell tests, NiRu/C 9:1 catalyst exhibited a high performance, reaching a current density of 2 A cm^{-2} at 1.95 V. This outperformed most reported results from literature using Pt/C cathodes tested in comparable conditions (table S2). In this study, the NiRu/C 9:1 catalyst-based cell showed comparable performance with the Pt/C based reference cell. In more insight into HFR corrected polarization curves, NiRu/C 9:1 catalyst showed better activity at current densities above 0.75 A cm^{-2}. With this performance, we consider NiRu/C catalysts to be promising as cost-effective substitution of Pt/C for future AEMWE applications. It should be noted that catalysts synthesized in this work are not yet completely structurally optimized as some large Ni particles are present. This also reveals potential for optimization in future studies. Furthermore, the long-term stability of this material needs to be investigated (while simultaneously optimizing operation parameters like KOH concentration and CL morphology) in full MEA set-ups to examine its practical applicability.

Data availability statement

All data that support the findings of this study are included within the article (and any supplementary files).

Acknowledgments

We acknowledge the support from the National Research Council of Canada's (NRC-CNRC) National Program Office and Materials for Clean Fuels Challenge Program for the joint project between the NRC-CNRC and HI ERN. Furthermore, the project partners from NRC Vancouver for accommodation in their facility and the joint work on this project. Special thanks to the time consuming TEM and SEM analysis of A Körner, A Hutzler and M Bierling and the enriching discussions with all colleagues and supervisors at HI-ERN. A Körner and A Hutzler gratefully acknowledge financial support by the Federal Ministry of Education and Research (BMBF) via the project H_2Giga—StacIE (Grant No. 03HY103H).

Conflict of interest

The authors declare no conflict of interest.

ORCID iD

S Ruck https://orcid.org/0000-0003-1018-0941

References

[1] Ball M and Weeda M 2015 The hydrogen economy—vision or reality? *Int. J. Hydrog. Energy* **40** 7903–19
[2] Turner J A 2004 Sustainable hydrogen production *Science* **305** 972–4
[3] Rosen M A and Koohi-Fayegh S 2016 The prospects for hydrogen as an energy carrier: an overview of hydrogen energy and hydrogen energy systems *Energy Ecol. Environ.* **1** 10–29
[4] Züttel A, Remhof A, Borgschulte A and Friedrichs O 2010 Hydrogen: the future energy carrier *R. Soc.* **368** 3329–42
[5] Kraglund M R 2017 Alkaline membrane water electrolysis with non-noble catalysts *Dissertation* Technical Univeristy of Denmark, Lyngby
[6] Vincent I and Bessarabov D 2018 Low cost hydrogen production by anion exchange membrane electrolysis: a review *Renew. Sustain. Energy Rev.* **81** 1690–704
[7] Vincent I, Lee E-C and Kim H-M 2020 Highly cost-effective platinum-free anion exchange membrane electrolysis for large scale energy storage and hydrogen production *RSC Adv.* **10** 37429–38
[8] Arges C G and Zhang L 2018 Anion exchange membranes' evolution toward high hydroxide ion conductivity and alkaline resiliency *ACS Appl. Energy Mater.* **1** 2991–3012
[9] Du N, Roy C, Turnbull M, Peach R, Thiele S and Bock C 2022 Alkaline anion exchange membrane electrolyzers: progress, gaps and future targets *Chem. Rev.* **122** 11830–95

[10] Shiva Kumar S and Himabindu V 2019 Hydrogen production by PEM water electrolysis—a review *Mater. Sci. Energy Technol.* **2** 442–54
[11] Recent M M 2021 Advancement on anion exchange membranes for fuel cell and water electrolysis *ChemElectroChem* **8** 36–45
[12] Hansen J N, Prats H, Toudahl K K, Mørch Secher N, Chan K, Kibsgaard J and Chorkendorff I 2021 Is there anything better than Pt for HER? *ACS Energy Lett.* **6** 1175–80
[13] Kibsgaard J and Chorkendorff I 2019 Considerations for the scaling-up of water splitting catalysts *Nat. Energy* **4** 430–3
[14] Vesborg P C K and Jaramillo T F 2012 Addressing the terawatt challenge: scalability in the supply of chemical elements for renewable energy *RSC Adv.* **2** 7933
[15] Wang J, Gao Y, Kong H, Kim J, Choi S, Ciucci F, Hao Y, Yang S, Shao Z and Lim J 2020 Non-precious-metal catalysts for alkaline water electrolysis: operando characterizations, theoretical calculations, and recent advances *Chem. Soc. Rev.* **49** 9154–96
[16] Yu F, Yu L, Mishra I K, Yu Y, Ren Z F and Zhou H Q 2018 Recent developments in earth-abundant and non-noble electrocatalysts for water electrolysis *Mater. Today Phys.* **7** 121–38
[17] Gong M, Wang D-Y, Chen C-C and Hwang B-J D H 2016 A mini review on nickel-based electrocatalysts for alkaline hydrogen evolution reaction *Nano Res.* **9** 28–46
[18] Greeley J, Jaramillo T F, Bonde J, Chorkendorff I B and Nørskov J K 2006 Computational high-throughput screening of electrocatalytic materials for hydrogen evolution *Nat. Mater.* **5** 909–13
[19] Faid A Y, Barnett A O, Seland F and Sunde S 2021 NiCu mixed metal oxide catalyst for alkaline hydrogen evolution in anion exchange membrane water electrolysis *Electrochim. Acta* **371** 137837
[20] Faid A, Oyarce Barnett A, Seland F and Sunde S 2018 Highly active nickel-based catalyst for hydrogen evolution in anion exchange membrane electrolysis *Catalysts* **8** 614
[21] Wei J, Zhou M, Long A, Xue Y, Liao H, Wei C and Xu Z J 2018 Heterostructured electrocatalysts for hydrogen evolution reaction under alkaline conditions *Nanomicro Lett.* **10** 75
[22] Ye C, Zhang L, Yue L, Deng B, Cao Y, Liu Q, Luo Y, Lu S, Zheng B and Sun X 2021 A NiCo LDH nanosheet array on graphite felt: an efficient 3D electrocatalyst for the oxygen evolution reaction in alkaline media *Inorg. Chem. Front.* **8** 3162–6
[23] Chen J G, Menning C A and Zellner M B 2008 Monolayer bimetallic surfaces: experimental and theoretical studies of trends in electronic and chemical properties *Surf. Sci. Rep.* **63** 201–54
[24] Yang Y, Lun Z, Xia G, Zheng F, He M and Chen Q 2015 Non-precious alloy encapsulated in nitrogen-doped graphene layers derived from MOFs as an active and durable hydrogen evolution reaction catalyst *Energy Environ. Sci.* **8** 3563–71
[25] Peng Z *et al* 2020 Surface engineering on nickel-ruthenium nanoalloys attached defective carbon sites as superior bifunctional electrocatalysts for overall water splitting *ACS Appl. Mater. Interfaces* **12** 13842–51
[26] Yuan L *et al* 2020 A general route to prepare low-ruthenium-content bimetallic electrocatalysts for pH-universal hydrogen evolution reaction by using carbon quantum dots *Angew. Chem.* **132** 1735–43
[27] Sun C, Zhao P, Yang Y, Li Z and Sheng W 2022 Lattice oxygen-induced *d*-band shifting for enhanced hydrogen oxidation reaction on nickel *ACS Catal.* **12** 11830–7
[28] Chalgin A, Song C, Tao P, Shang W, Deng T and Wu J 2020 Effect of supporting materials on the electrocatalytic activity, stability and selectivity of noble metal-based catalysts for oxygen reduction and hydrogen evolution reactions *Prog. Nat. Sci.: Mater. Int.* **30** 289–97
[29] Xue Y, Shi L, Liu X, Fang J, Wang X, Setzler B P, Zhu W, Yan Y and Zhuang Z 2020 A highly-active, stable and low-cost platinum-free anode catalyst based on RuNi for hydroxide exchange membrane fuel cells *Nat. Commun.* **11** 5651
[30] Li M, Wang H, Zhu W, Li W, Wang C and Lu X 2020 RuNi nanoparticles embedded in N-doped carbon nanofibers as a robust bifunctional catalyst for efficient overall water splitting *Adv. Sci.* **7** 1901833
[31] Liu J, Wang C, Rong F, Wu S, Tian K, Wang M, He L, Zhang Z and Du M 2020 Nickel-ruthenium nanoalloy encapsulated in mesoporous carbon as active electrocatalysts for highly efficient overall water splitting in alkaline solution *Electrochim. Acta* **334** 135653
[32] Lazaridis T, Stühmeier B M, Gasteiger H A and El-Sayed H A 2022 Capabilities and limitations of rotating disk electrodes versus membrane electrode assemblies in the investigation of electrocatalysts *Nat. Catal.* **5** 363–73
[33] Yin H, Zhao S, Zhao K, Muqsit A, Tang H, Chang L, Zhao H, Gao Y and Tang Z 2015 Ultrathin platinum nanowires grown on single-layered nickel hydroxide with high hydrogen evolution activity *Nat. Commun.* **6** 6430
[34] Mayerhöfer B, Ehelebe K, Speck F D, Bierling M, Bender J, Kerres J A, Mayrhofer K J J, Cherevko S, Peach R and Thiele S 2021 On the effect of anion exchange ionomer binders in bipolar electrode membrane interface water electrolysis *J. Mater. Chem.* A **9** 14285–95
[35] Bühler M, Hegge F, Holzapfel P, Bierling M, Suermann M, Vierrath S and Thiele S 2019 Optimization of anodic porous transport electrodes for proton exchange membrane water electrolyzers *J. Mater. Chem.* A **7** 26984–95
[36] Pingali K C, Deng S and Rockstraw D A 2005 Synthesis of binary metal nanoparticles of Ru-Ni with core and shell structure *05AIChE: 2005 AIChE Annual Meeting and Fall Showcase* (*Cincinnati, OH, United States*, *30 October–4 November 2005*) pp 2687–706
[37] Rahman M M *et al* 2021 Synthesis of catalysts with fine platinum particles supported by high-surface-area activated carbons and optimization of their catalytic activities for polymer electrolyte fuel cells *RSC Adv.* **11** 20601–11
[38] Richardson J 2003 X-ray diffraction study of nickel oxide reduction by hydrogen *Appl. Catal. A: Gen.* **246** 137–50
[39] Clendenen R L and Drickamer H G 1964 The effect of pressure on the volume and lattice parameters of ruthenium and iron *J. Phys. Chem. Solids* **25** 865–8
[40] Bai X, Pang Q-Q, Du X, Yi S-S, Zhang S, Qian J, Yue X-Z and Liu Z-Y 2021 Integrating RuNi alloy in S-doped defective carbon for efficient hydrogen evolution in both acidic and alkaline media *Chem. Eng. J.* **417** 129319
[41] Koch S, Heizmann P A, Kilian S K, Britton B, Holdcroft S, Breitwieser M and Vierrath S 2021 The effect of ionomer content in catalyst layers in anion-exchange membrane water electrolyzers prepared with reinforced membranes (Aemion+™) *J. Mater. Chem.* A **9** 15744–54
[42] Ghoshal S, Pivovar B S and Alia S M 2021 Evaluating the effect of membrane-ionomer combinations and supporting electrolytes on the performance of cobalt nanoparticle anodes in anion exchange membrane electrolyzers *J. Power Sources* **488** 229433
[43] Zeng K and Zhang D 2010 Recent progress in alkaline water electrolysis for hydrogen production and applications *Prog. Energy Combust. Sci.* **36** 307–26
[44] Henkensmeier D, Najibah M, Harms C, Žitka J, Hnát J and Bouzek K 2021 Overview: state-of-the art commercial membranes for anion exchange membrane water electrolysis *J. Electrochem. Energy Convers. Storage* **18** 2

[45] Razmjooei F, Liu T, Azevedo D A, Hadjixenophontos E, Reissner R, Schiller G, Ansar S A and Friedrich K A 2020 Improving plasma sprayed Raney-type nickel-molybdenum electrodes towards high-performance hydrogen evolution in alkaline medium *Sci. Rep.* **10** 10948
[46] Park J E, Kang S Y, Oh S-H, Kim J K, Lim M S, Ahn C-Y, Cho Y-H and Sung Y-E 2019 High-performance anion-exchange membrane water electrolysis *Electrochim. Acta* **295** 99–106
[47] Chen P and Hu X 2020 High-efficiency anion exchange membrane water electrolysis employing non-noble metal catalysts *Adv. Energy Mater.* **10** 2002285